7. Flow turbulence and scouring process

7.1 Evolution of turbulent structures

The analyses performed in the previous chapters have allowed us to better understand how the knowledge of flow velocity field and turbulence characteristics is important to identify the scouring process downstream the rigid bed. In particular, the analysis of the Reynolds momentum flux components have suggested that the turbulent activity of flow seems to increase where the scour hole develops.

In this part of the work, the formation of the coherent turbulent structures inside the scour hole has been investigated. The conditioned quadrant analysis (Lu and Willmarth, 1973; Nezu and Nakagawa, 1993) has been applied to investigate about the role of turbulent processes on scouring mechanisms downstream the rigid bed.

Then, the values of the longitudinal Reynolds momentum flux have been used to estimate the bed shear stress distribution.

7.1.1 Quadrant analysis and occurrence frequency of events

The conditioned quadrant analysis consists in analyzing the sign of the instantaneous Reynolds momentum flux. On the basis of the observation discussed in the previous chapter, the quadrant analysis has been conducted only considering the Reynolds momentum flux component $\overline{u'_x u'_z}$. Negative values of the instantaneous products $u'_x(t) \cdot u'_z(t)$ correspond to ejection and sweep events: ejection occurs when low-speed fluid motions ($u'_x(t) < 0$) go away from the wall ($u'_z(t) > 0$); sweep event occurs when high-speed fluid ($u'_x(t) > 0$) moves toward the wall ($u'_z(t) < 0$). Positive values of the instantaneous products $u'_x(t) \cdot u'_z(t)$ correspond to inward and outward interactions: inward

interaction occurs when by low-speed fluid ($u_x'(t) < 0$) moves toward the wall ($u_z'(t) < 0$); outward interaction occurs when high-speed fluid motion ($u_x'(t) > 0$) arises far from the wall ($u_z'(t) > 0$). Both ejection and sweep events are related to turbulent energy production; outward and inward interactions determine energy dissipation (Pope, 2000).

Thus, the instantaneous plane $[u_x'(t) - u_z'(t)]$ has been divided into four quadrants, so that each quadrant represents on average a turbulent event. Quadrant I represents outward interaction event ($u_x'(t) > 0$ and $u_z'(t) > 0$); quadrant II indicates ejection event ($u_x'(t) < 0$ and $u_z'(t) > 0$); quadrant III represents inward interaction event ($u_x'(t) < 0$ and $u_z'(t) < 0$); quadrant IV defines sweep event ($u_x'(t) > 0$ and $u_z'(t) < 0$).

For example the scatter plots of two measurement points located at section X5 (both at a distance of 0.8 cm from the bed), respectively for Y = 4cm and Y = 21cm, are reported in Figure 7.1.

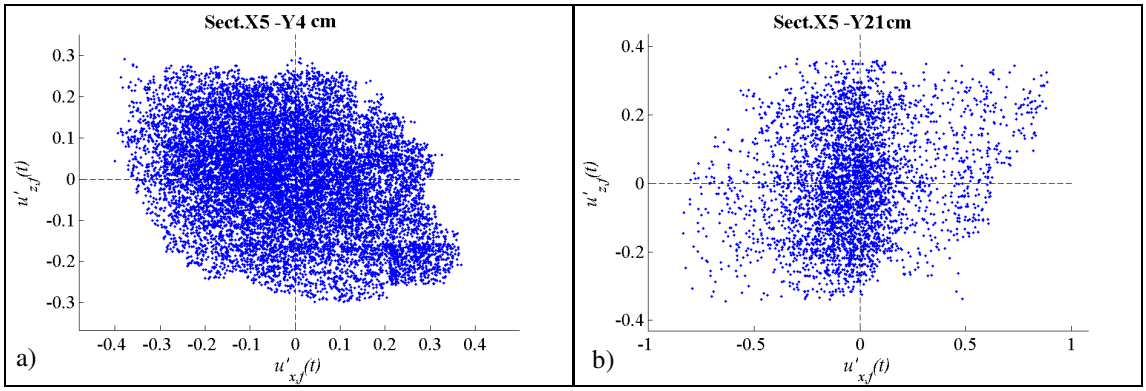

Figure 7.1 – Scatter plot of couples $[u_x'(t), u_z'(t)]$: a) Y = 4cm; b) Y = 21cm.

According to previous works (Nezu and Nakagawa, 1993; Cellino and Lemmin, 2004), in order to isolate the contribution of extreme events within each quadrant, a hyperbolic

excluding hole has been defined on the instantaneous plane $\left[u_x'(t) - u_z'(t)\right]$ that is bounded by the curves:

$$\left|u_x'(t) \cdot u_z'(t)\right| = q \cdot \sqrt{\overline{u_x'(t)}^2}\sqrt{\overline{u_z'(t)}^2} \tag{7.1}$$

where q represents the threshold level and the over-bar indicates the time-averaged value. Such filtering analysis allow us to separate background turbulence from large magnitude events (Bey et al., 2007). In general, the determination of q is more or less arbitrary. Furthermore, high values of the threshold level q allow to select stronger events, but, as consequence, the corresponding contributing region diminishes and the total number of couples $[u_x'(t), u_z'(t)]$ considered for the analysis could be strongly reduced.

In this work 10 different threshold levels q varying in the range q = 0.2 ÷ 2 (with a step of 0.2) have been investigated. The excluding holes corresponding to some of the aforementioned threshold levels (q = 0.2÷2.0, with a step of 0.6) are shown in Figure 7.2.

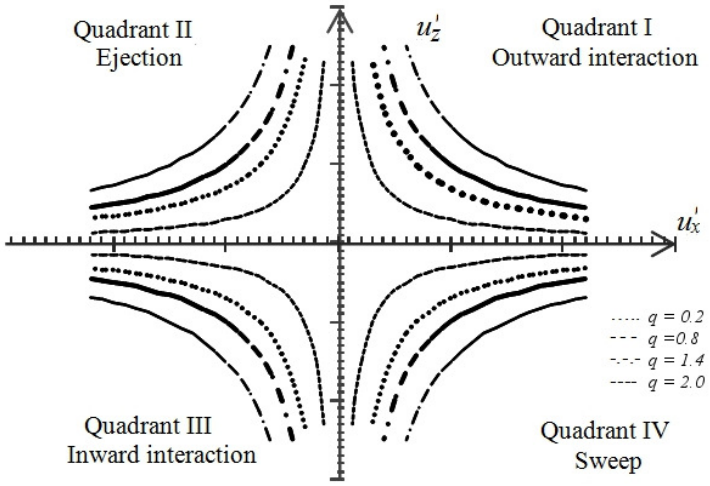

Figure 7.2 – Excluding hole regions.

Thus, for each measurement point, the instantaneous Reynolds momentum flux $u_x'(t)u_z'(t)$ have been filtered by a discriminating function $I_k(t)$ (where the index k = I, II,

III, IV indicates the quadrant where the generic event falls and t is the time). Thus, for each event, the discriminating function is defined as:

$$I_k(t) = \begin{cases} 1, \text{ if the couple } [u_x'(t), u_z'(t)] \text{ falls in the } k\text{ - th quadrant} \\ 0, \text{ otherwise} \end{cases} \tag{7.2}$$

The discriminating functions defined by (7.2) allow the identification of the regions contributing to each turbulent event. The dimension of such regions and, thus, of the corresponding excluding hole, depends on the value of the threshold level q.

For each measurement point, the occurrence frequency of the event falling in *k-th* quadrant, f_k (k = I, II, III, IV) has been estimated for each considered threshold level q as:

$$f_k = \frac{\sum_{t=0}^{T} I_k(t)}{\sum_{t=0}^{T} I_I(t) + \sum_{t=0}^{T} I_{II}(t) + \sum_{t=0}^{T} I_{III}(t) + \sum_{t=0}^{T} I_{IV}(t)} \tag{7.3}$$

where T is the measurement time length. Thus, in order to identify the best value of the threshold level, a statistic analysis has been performed for measurement points located at distance of 0.8cm from the bed (number of the considered points N_s = 363). Furthermore, for each threshold level q, the rate of the residual samples $r_{q,i}$ has been also calculated at each considered measurement point as:

$$r_{q,i} = \frac{N_{q,i}}{N_{0,i}},\ i = 1,\ldots,N_s \tag{7.4}$$

where $N_{0,i}$ and $N_{q,i}$ are the number of couples $[u_x'(t), u_z'(t)]$, respectively, the initial (with q = 0) and the residual for the threshold level q for the *i-th* measurement point. Thus the average value, $R(q)$, of $r_{q,i}$ for the considered threshold level q has been calculated as:

$$R(q) = \frac{\sum_{i=1}^{Ns} r_{q,i}}{N_s} \cdot 100 \tag{7.5}$$

In order to estimate the goodness of each considered threshold level q, the difference between the relative frequency of the upward events, $c_{up}(q,i)=\left|\left[f_I(q,i)-f_{II}(q,i)\right]\right|$, and the difference between the relative frequency of the of downward events, $c_{down}(q,i)=\left|\left[f_{III}(q,i)-f_{IV}(q,i)\right]\right|$, have been calculated for each measurement point. Consequently the average values $C_{up}(q)$ and $C_{down}(q)$, respectively of the coefficients $c_{up}(q,i)$ and $c_{down}(q,i)$, are determined as:

$$\begin{cases} C_{up}(q)=\dfrac{\sum_{i=1}^{Ns} c_{up}(q,i)}{N_s} \\ C_{down}(q)=\dfrac{\sum_{i=1}^{Ns} c_{down}(q,i)}{N_s} \end{cases}; \tag{7.6}$$

These three coefficients, $R(q)$, $C_{up}(q)$ and $C_{down}(q)$, have been plotted versus the considered threshold level q in Figure 7.3.

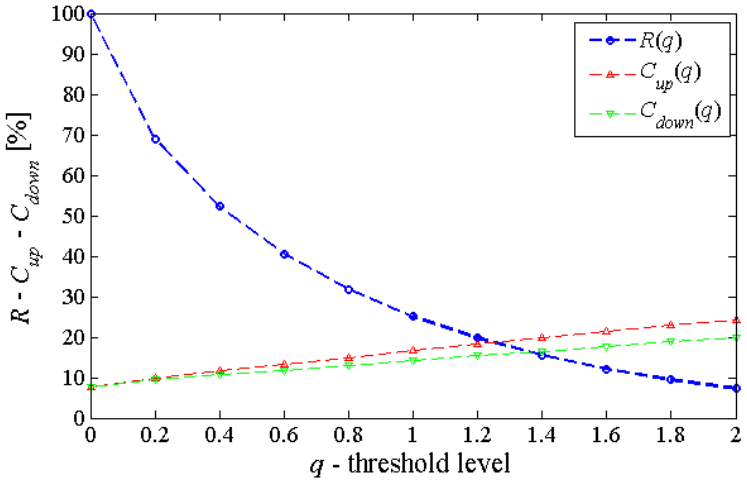

Figure 7.3 – Plots of $R(q)$, $C_{up}(q)$ and $C_{down}(q)$ versus the threshold level q.

Figure 7.3 shows that high values of the threshold level q allow one to select stronger events and to clearly distinguish the frequency of occurrence of each event, but, as

consequence, the total number of couples $[u'_x(t), u'_z(t)]$ considered for the analysis could be strongly reduced. For q = 0 the events are not clearly distinguishable ($C_{up}(2) \cong C_{down}(2) <$ 10%). For q = 2 it can be seen a strong reduction of the number of couples (the residual couples $[u'_x(t), u'_z(t)]$ are $R(2) <10\%$) , while the events are clearly distinguishable ($C_{up}(2) \cong C_{down}(2) \cong 20\%$). For an intermediate threshold level (q = 0.8÷1.0) the events are still distinguishable ($[C_{up}(q) \cong C_{down}(q)]_{q=0.8\div1} \cong 13 \div 15\ \%$) and the residual of turbulent fluctuation couples $[u'_x(t), u'_z(t)]$ is $R(q) = 20 \div 32\ \%$.

Thus the threshold level q = 0.8 has been considered as a good compromise between a clear distinction of the events ($C_{up}(0.8) \cong C_{down}(0.8) \cong 13\%$) and an acceptable number of considered couples ($R(0.8)=32\%$) .

On the basis of this results, the instantaneous turbulent fluctuation components $[u'_x(t), u'_z(t)]$ have been filtered by excluding the points falling inside the excluding hole identified by the threshold level q = 0.8. The quadrant analysis has been performed by considering the filtered time series given by:

$$\begin{cases} \left[u'_{x,f}(t), u'_{z,f}(t)\right] = \left|u'_{x,f}(t) \cdot u'_{z,f}(t)\right| \cdot I_k(t) > q \cdot \sqrt{\overline{u'_{x,f}(t)^2}} \cdot \sqrt{\overline{u'_{z,f}(t)^2}} \\ q = 0.8 \end{cases} \tag{7.7}$$

Here on the filtered time series $\left[u'_{x,f}(t), u'_{z,f}(t)\right]$ will be simply indicated as $\left[u'_x(t), u'_z(t)\right]$. In order to identify the event occurring in each measurement point the histograms of the occurrence frequency f_k (k = I, II, III, IV) of events falling in the *k-th* quadrant, have been calculated. As an example the histograms relative to the measurement points with a distance of 0.8 cm from the bed are reported in Figure 7.4.

From this figure it can be observed that into the right bank region ejection and sweep events occur. In particular, in the deepest part of the scour hole (sections X5 and X10) ejections occur more frequently than sweep events. In the central region (see Figures 7.4c-

e) the number of events of inward and outward interactions increases starting from section X35. Moreover, inward and outward interaction events occur particularly at Y = 21 cm within the scour hole (X < X30, Figure 7.4d) with exception for section X10, where a sweep events occurs. In the left bank region (see Figures 7.4e-g) only events of II and IV quadrant occur. In particular the histograms show that ejection events are predominant (over 75%) over sweep events in sections for X = X10÷X20.

Thus, the aforementioned analysis has highlighted that in the near bank regions ejection and sweeps events occur; inward and outward interaction events occur essentially in the central region. In particular, ejection events are predominant over sweep events in the deepest part of the scour (bed slope is negative); sweep events occur more frequently in the remaining part of the scour hole (bed slope is positive). As previous works show (Williams and Kemp, 1971; Grass, 1971, 1983) sweeps are responsible for sediment transport over rough beds. Sweeps events (directed downward and towards the bed) lead to sediment being moved for a short distance along the bed.

In order to extend the analysis to the entire water depth, the probability of occurrence of each event has been calculated along each measurement vertical. The joint probability density function (JPDF) of the filtered couples $\left[u_x'(t), u_z'(t)\right]$, P_{xz}, has been estimated as (Pope, 2000):

$$P_{xz} = A_{xz} \cdot \exp\left[B_{xz} \cdot \left(\frac{u_x'(t)^2}{\overline{u_x'(t)^2}} - 2 \cdot \frac{\rho_{xz} \cdot u_x'(t) \cdot u_z'(t)}{\left[\overline{u_x'(t)^2} \ \overline{u_z'(t)^2} \right]^{1/2}} + \frac{u_z'(t)^2}{\overline{u_z'(t)^2}} \right) \right]$$

where

$$A_{xz} = \left[4\pi^2 \cdot \overline{u_x'(t)^2} \ \overline{u_z'(t)^2} \cdot \left(1 - \rho_{xz}^2\right) \right]^{-1/2} \tag{7.8}$$

$$B_{xz} = \frac{-0.5}{1 - \rho_{xz}^2}$$

$$\rho_{12} = \overline{u_x'(t) \cdot u_z'(t)} \cdot \left[\overline{u_x'(t)^2} \ \overline{u_z'(t)^2} \right]^{-1/2}$$

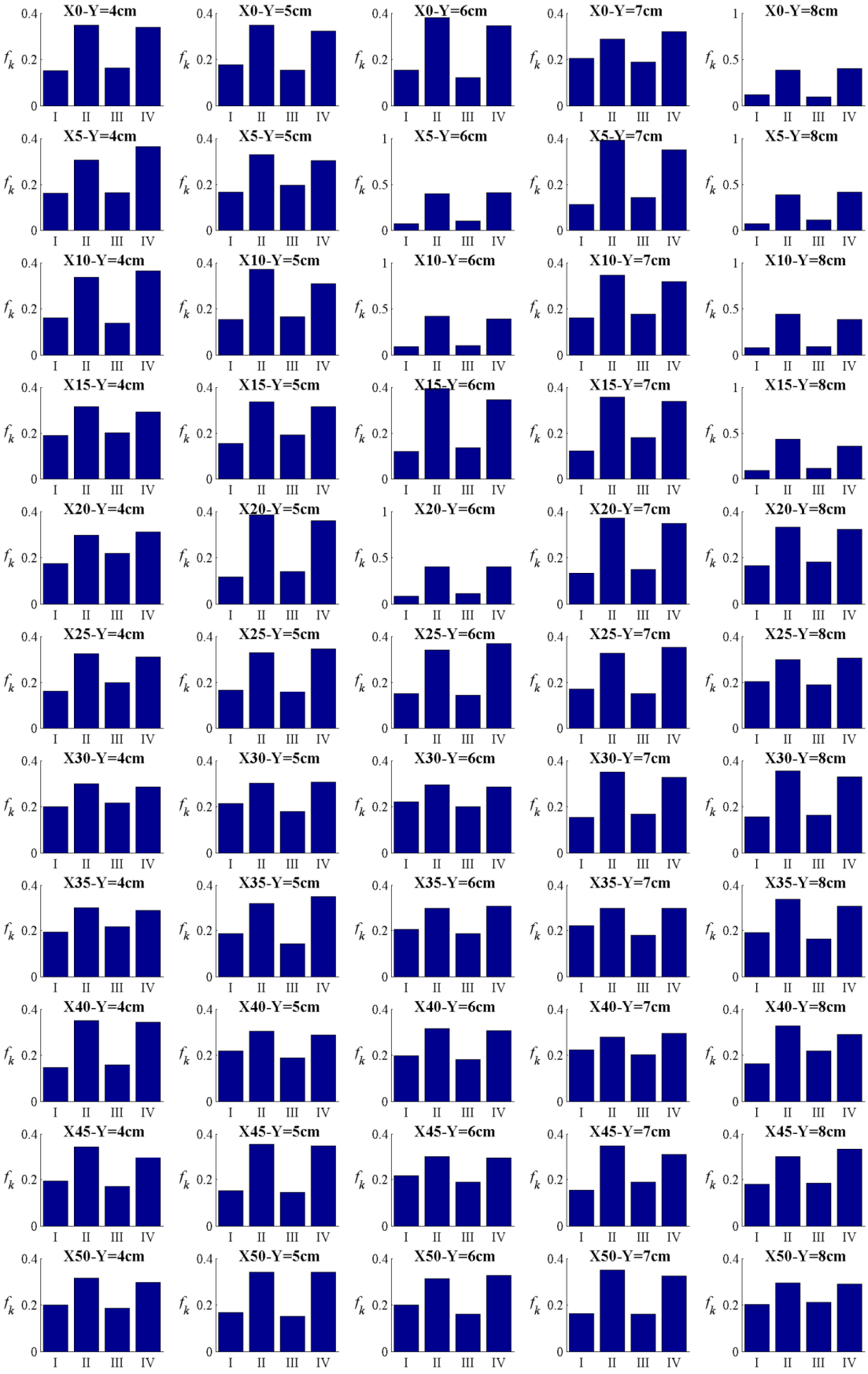

Figure 7.4 – Histograms of turbulent events frequency: a) 4cm < Y < 8cm.

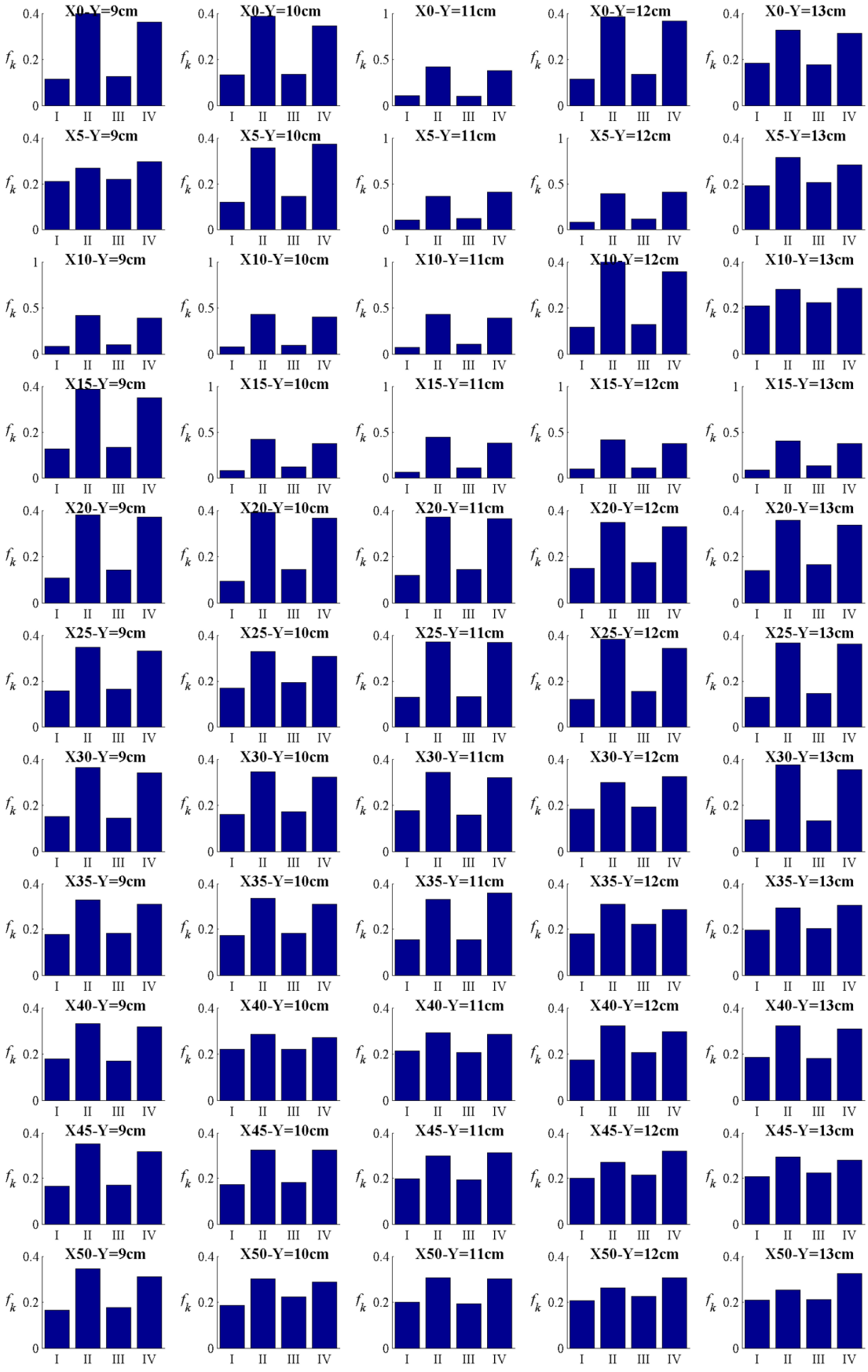

Figure 7.4 – Histograms of turbulent events frequency: b) 9cm < Y < 13cm.

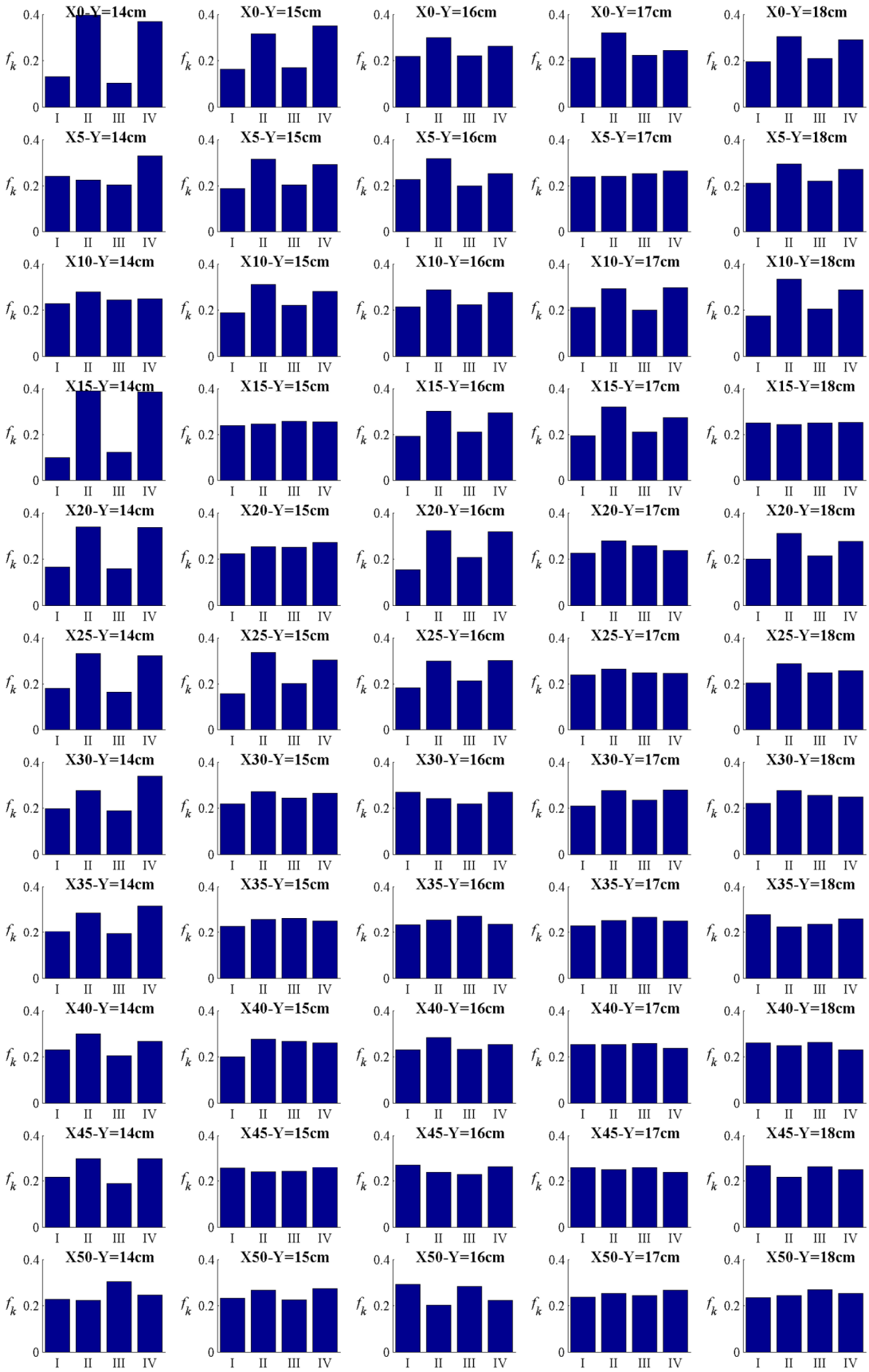

Figure 7.4 – Histograms of turbulent events frequency: c) 14cm < Y < 18cm.

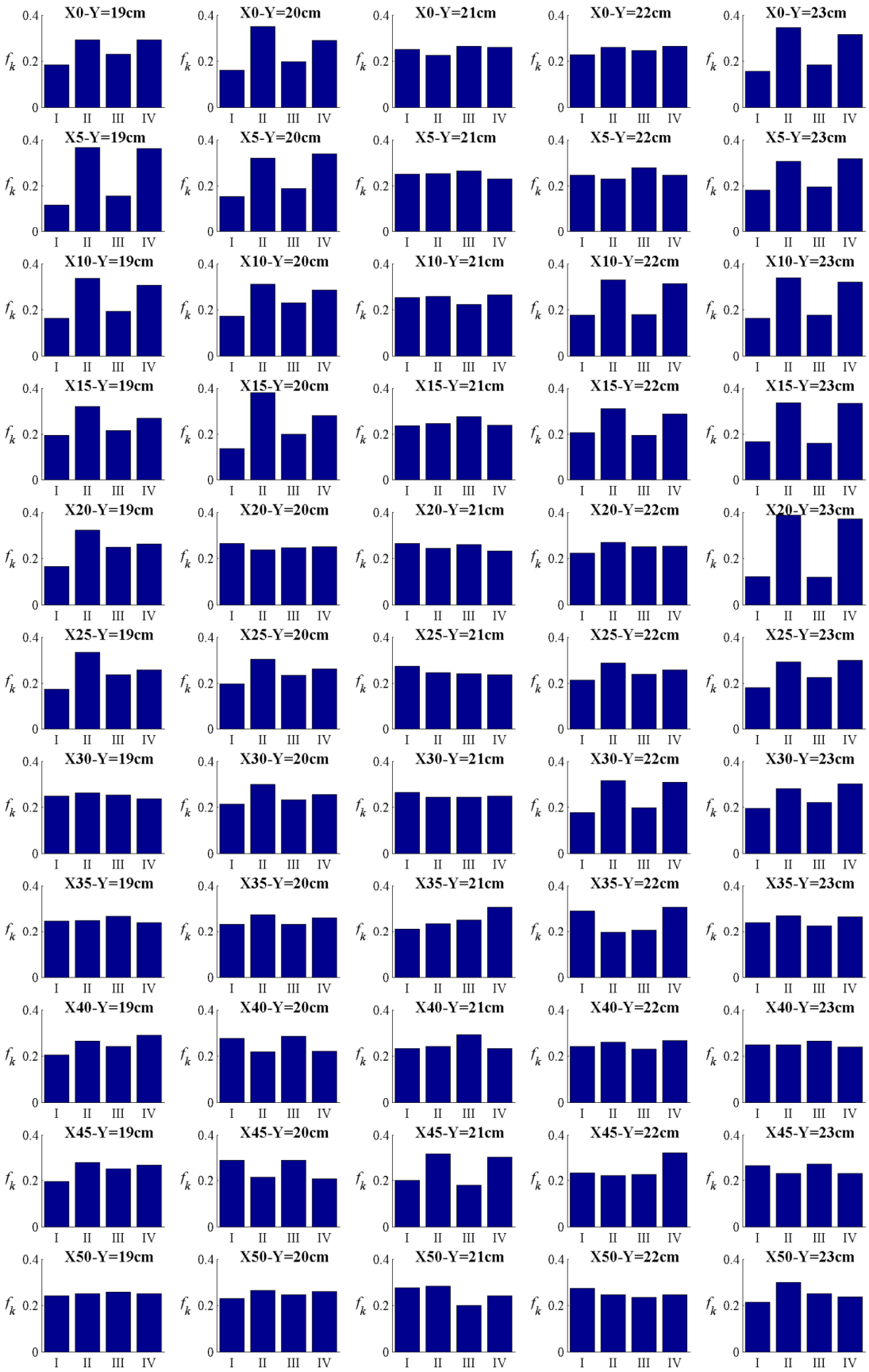

Figure 7.4 – Histograms of turbulent events frequency: d) 19cm < Y < 23cm.

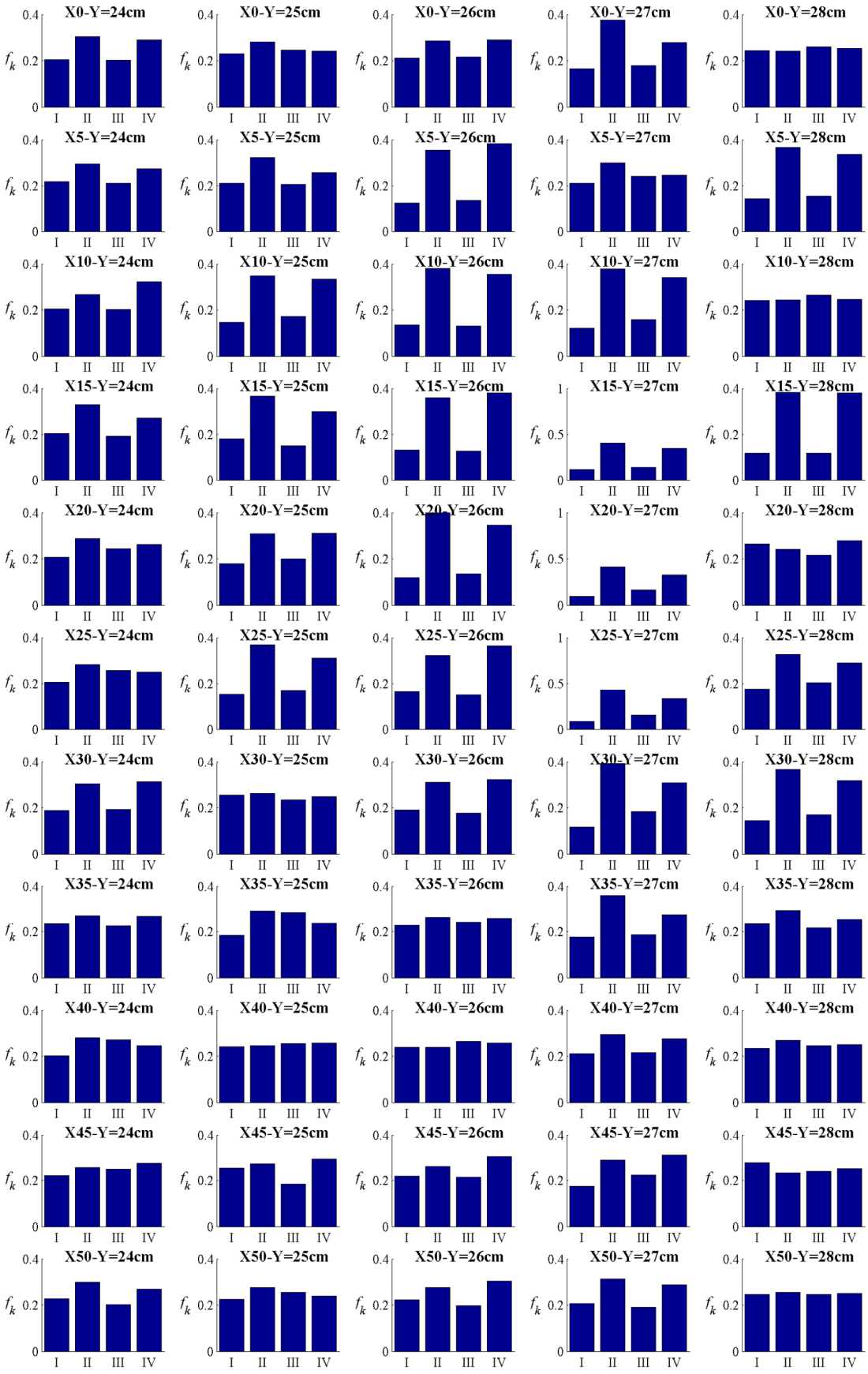

Figure 7.4 – Histograms of turbulent events frequency: e) 24cm < Y < 28cm.

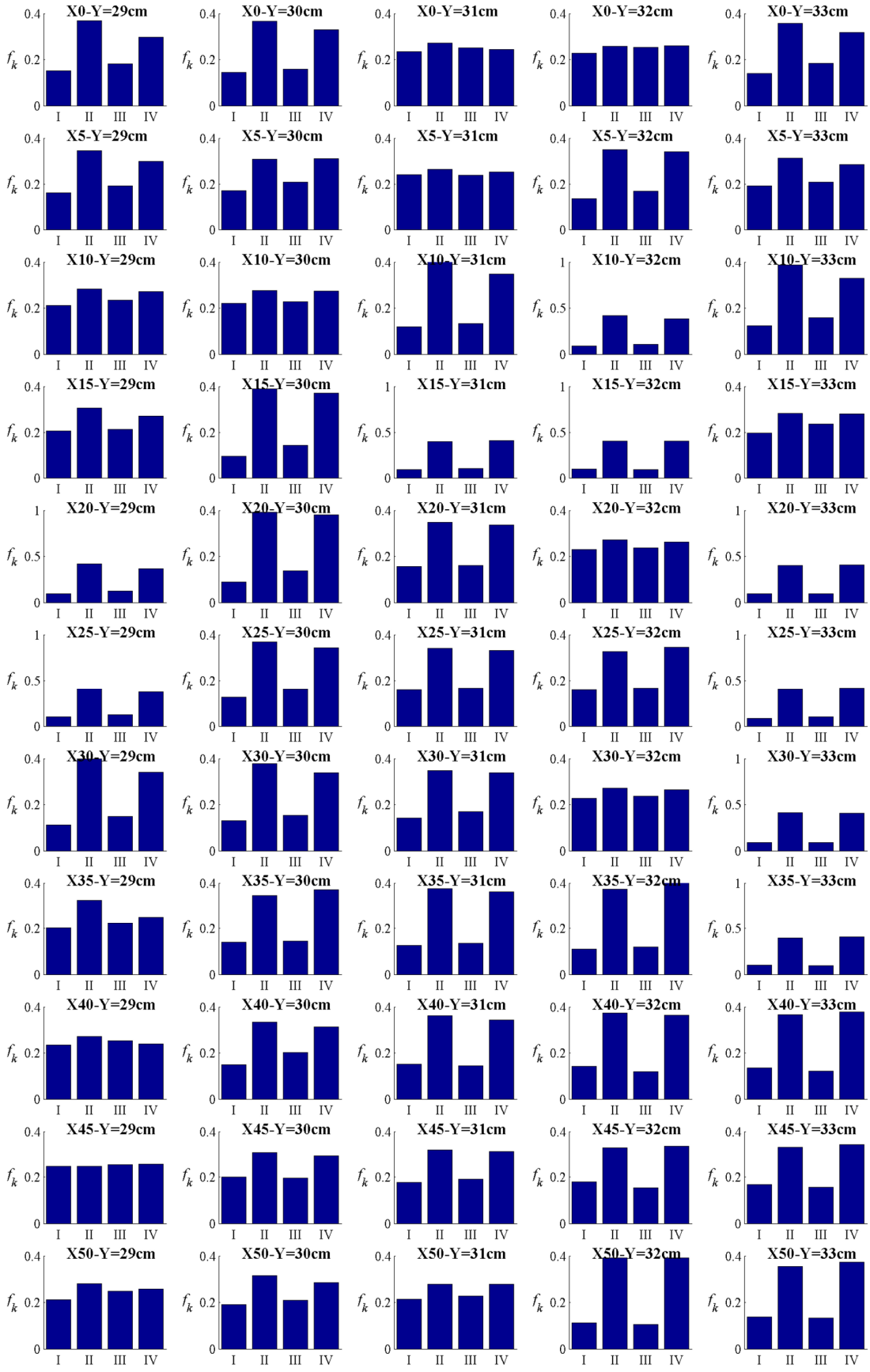

Figure 7.4 – Histograms of turbulent events frequency: f) 29cm < Y < 33cm.

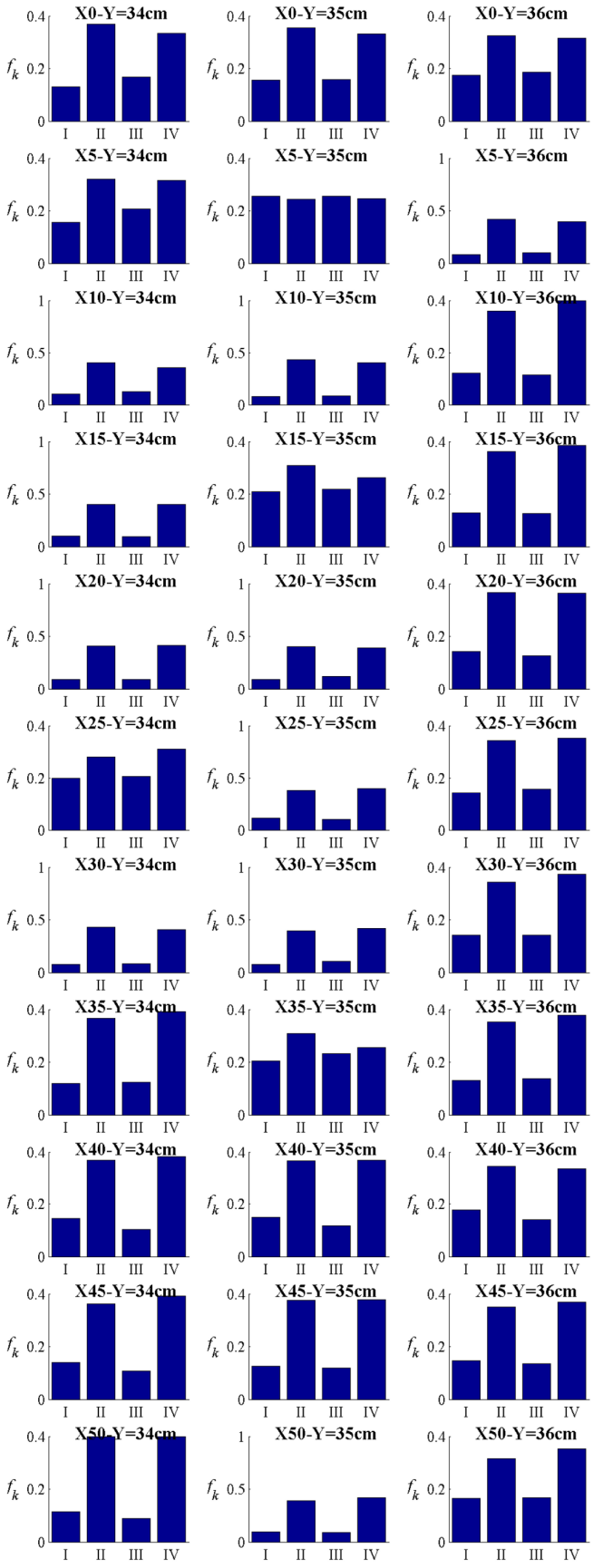

Figure 7.4 – Histograms of turbulent events frequency: g) 34cm < Y < 36cm.

The distribution of P_{xz} on the plane $\left[u_x'(t), u_z'(t)\right]$ is represented by an ellipse, whose long axis is rotated according to the more frequent event occurring in the considered measurement point. Figure 7.5 reports the distribution of P_{xz} in the measurement points along the verticals V1 = [X = 10 cm,Y = 4 cm], V2 = [X = 10 cm,Y = 21 cm] , V3 = [X = 15 cm,Y = 36 cm]. These verticals have been selected on the basis of the results shown in chapter 4. In particular, V1 and V3 are where the maximum scour depth occurs (Y = 4 cm and Y = 36 cm), V2 is at the central region, where deposit occurs. Along each examined vertical the mutual distance between the measurement point is equal to ΔZ = 6 mm.

In Figure 7.5 the contour plots of P_{xz} show that ejection and sweep events occur in both the near bank regions along the whole water depth. In the central region (X = 10 cm, Y = 21 cm) along the vertical direction inward and outward interaction events especially are found. In particular, near the bed (at a distance of 0.8 cm from the bed) ejection and sweep events occur. Approaching to the water surface, inward and outward interaction events occur. Thus, in the near bank regions, ejection and sweep events essentially occur in the whole water depth. In the central region, where erosion is not evident and flow velocity assumes low values (see Figure 5.6a), interaction events occur especially near the water surface; ejection and sweep events occur near to the bed, where high values of the Reynolds momentum fluxes have been also observed.

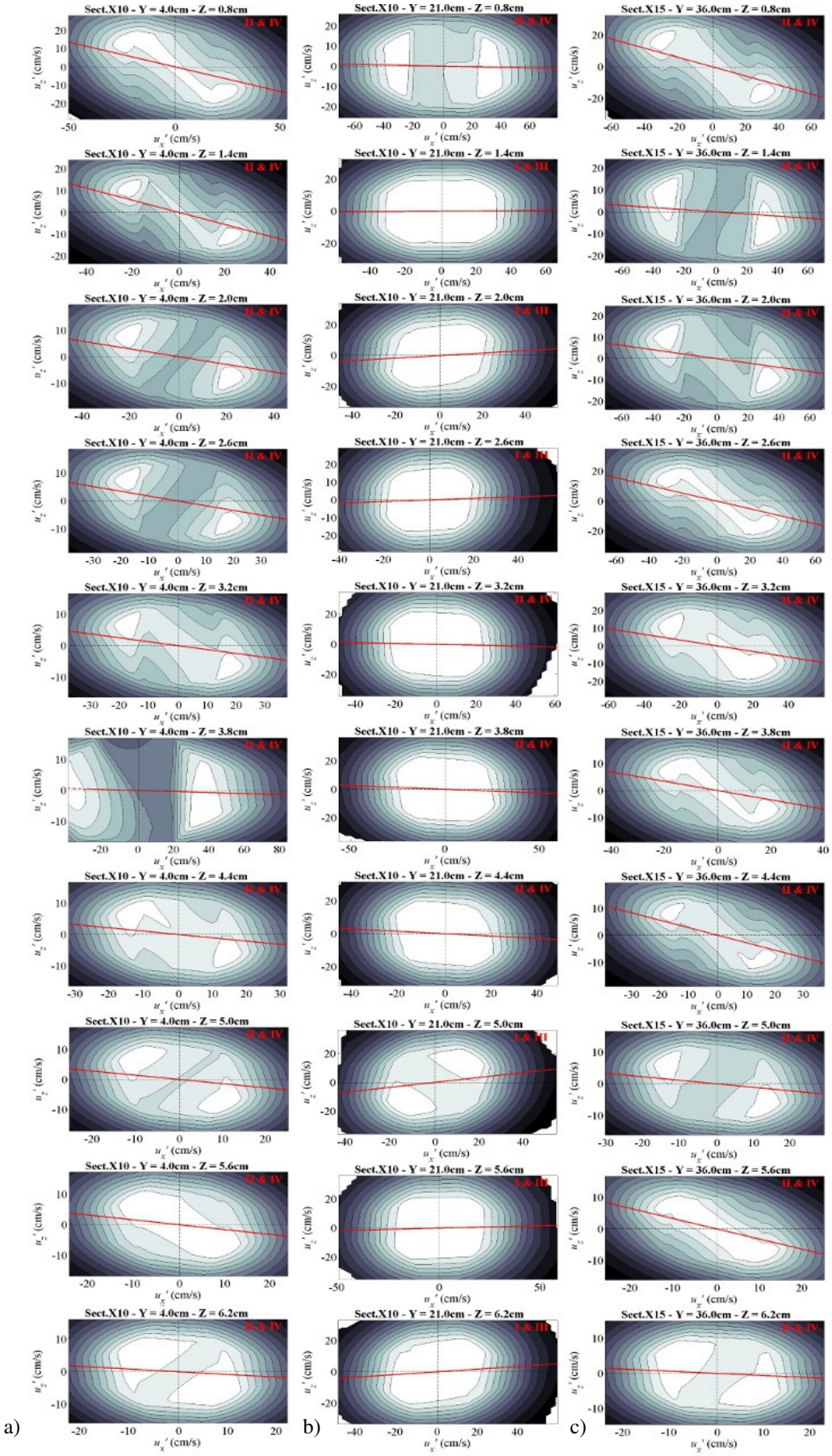

Figure 7.5 – Contour plots of P_{xz} :a) vertical V1; b) vertical V2; c) vertical V3.

7.2 Bed shear stress distribution

The distribution of the shear stress near the bed τ_b inside the scour hole has been estimated by using the values of the instantaneous experimental Reynolds momentum flux $u_x'(t)\,u_z'(t)$ described in chapter 6. Taking into account that (Bennet and Best, 1995; Graf, 1996):

$$\tau_b = \rho \cdot (u^*)^2 \cong \left(-\rho \cdot \overline{u_x'(t)\,u_z'(t)}\right)_{Z=Z_b} \qquad (7.9)$$

where u^* is the shear flow velocity near the bed, ρ is the water density, Z_b is the zero bed height and $\overline{u_x'(t)\,u_z'(t)}$ is the Reynolds momentum flux defined in equation 6.2.

Thus, the linear regression of the Reynolds stress, $-\rho \cdot \overline{u_x'(t)\,u_z'(t)}$, along each measurement vertical allowed us to evaluate τ_b as projection of the Reynolds momentum at Z_b.

The vertical distributions of the Reynolds momentum fluxes are reported in Figure 7.6. In this figure the interpolating line has been also reported. It can be observed that near the right bank and inside the scour hole (Y ≤ 18cm and X < X25, see Figures 7.6a-c), the Reynolds stress has a linear vertical trend near the free surface, but approaching to the bed the Reynolds shear stress increases in intensity assuming a peak value near the bed. In the right bank region the highest values of the Reynolds stress are found at section X10. Thus the highest peak value of the Reynolds stress is found where the scour is maximum. In the central region, the Reynolds shear stress assumes a linear almost vertical trend in the whole water depth. In the left bank region the vertical profiles of Reynolds stress (Figures 7.6f-g) show the same trend as observed near the right bank region. The highest values of the Reynolds shear stress are found for Y = 34cm at section X20 (Figure 7.6g).

Figure 7.7 shows the comparison between the bed shear stress estimated by equation 7.9 and the longitudinal bed profiles. From these figure it can be observed that the bed shear stress increases in value as the scour depth increases and vice-versa. In particular, the bed shear stress increases in the ranges Y < 10cm and X0 < X < X10 (Figures 7.7a-b).

At section X10 it assumes the highest value ($\tau_b \cong 30 N/m^2$). Then, for 11cm < Y < 15cm and X < X10 τ_b starts to reduce in value so that in the central region (see Figures 7.7c-d) it assumes low values ($\tau_b \cong 5\ N/m^2$). Where the bed slope inside the scour hole becomes positive (X10 < X < X30), τ_b generally increases in value. For X > X30 the bed shear stress τ_b assumes always low values. Approaching to the left bank region (Y > 26 cm) the shear stress increases again. At Y = 34 cm and at section X15, τ_b assumes the highest peak values ($\tau_b \cong 27\ N/m^2$). The distribution of the computed bed shear stress of τ_b is reported in Figure 7.8. This figure shows two positive peaks of the bed shear stress at section X10 for Y = 10 cm, and at section X15 for Y = 34 cm. These peak values occur where the scour depths assume high values. Moreover negative values of the bed shear stress are also distinguishable at the channel axis for X > X35.

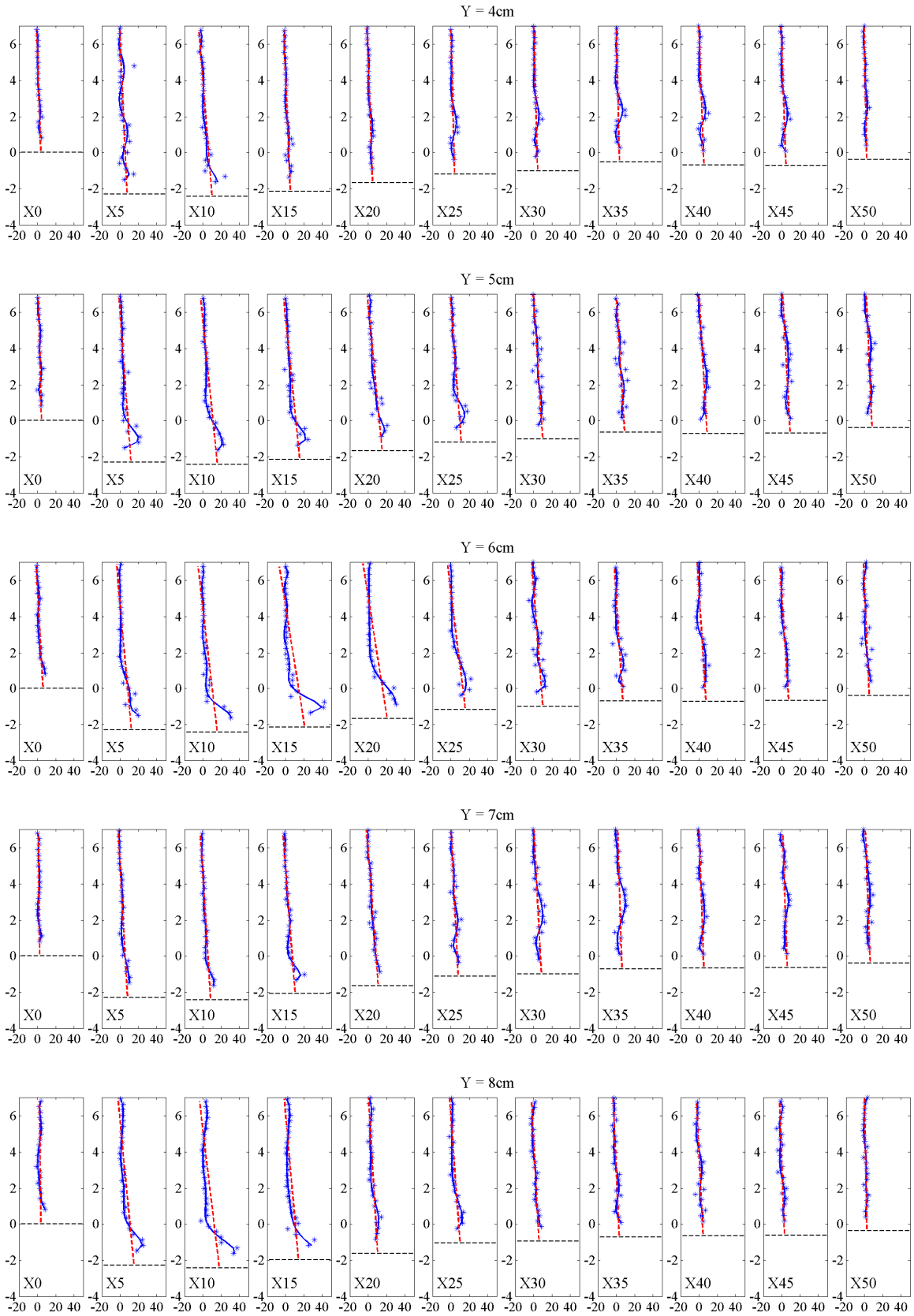

Figure 7.6 – Vertical distributions of the Reynolds stress (N/m^2): a) 4cm < Y < 8cm.

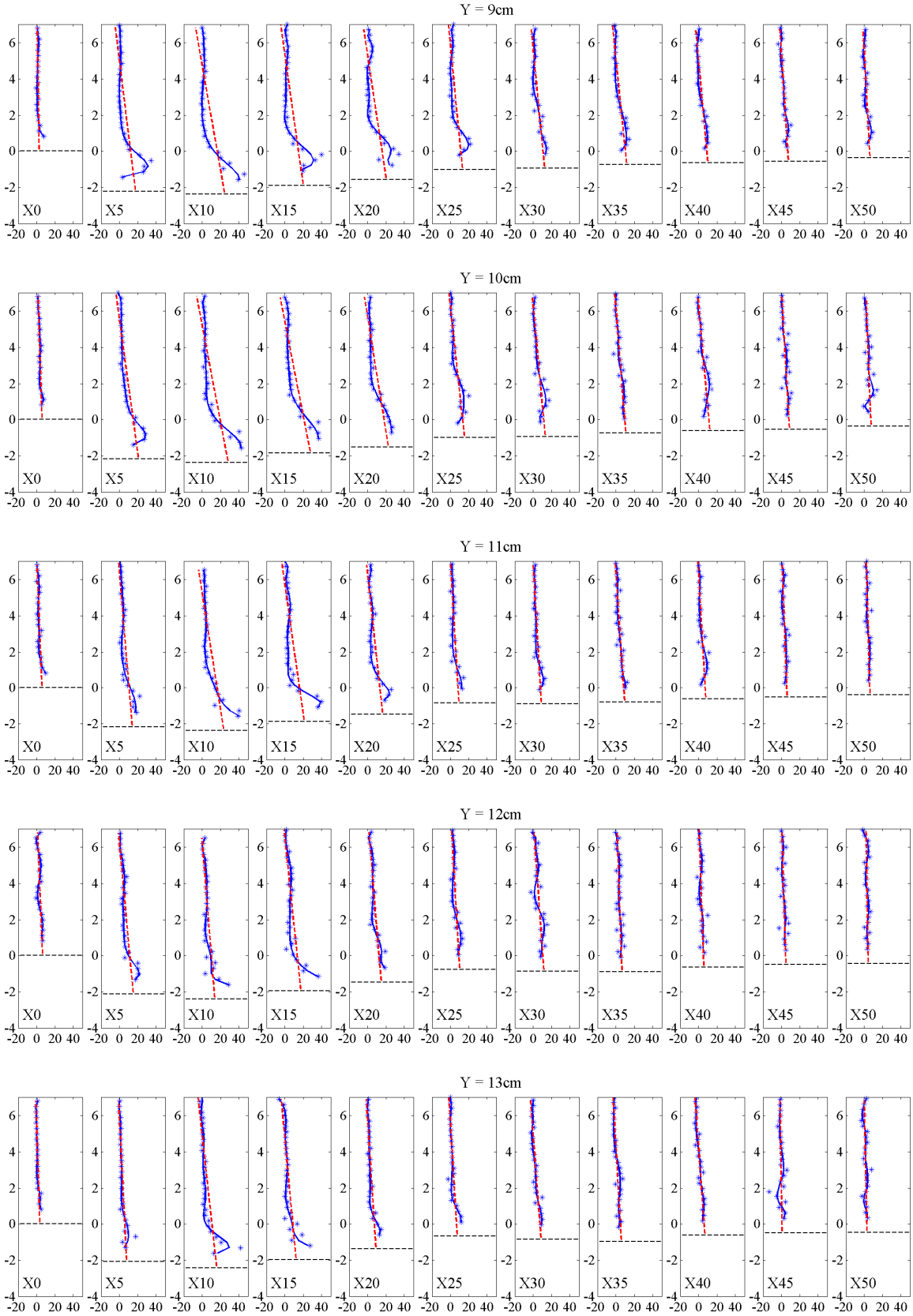

Figure 7.6 – Vertical distributions of the Reynolds stress (N/m^2): b) 9cm < Y < 13cm.

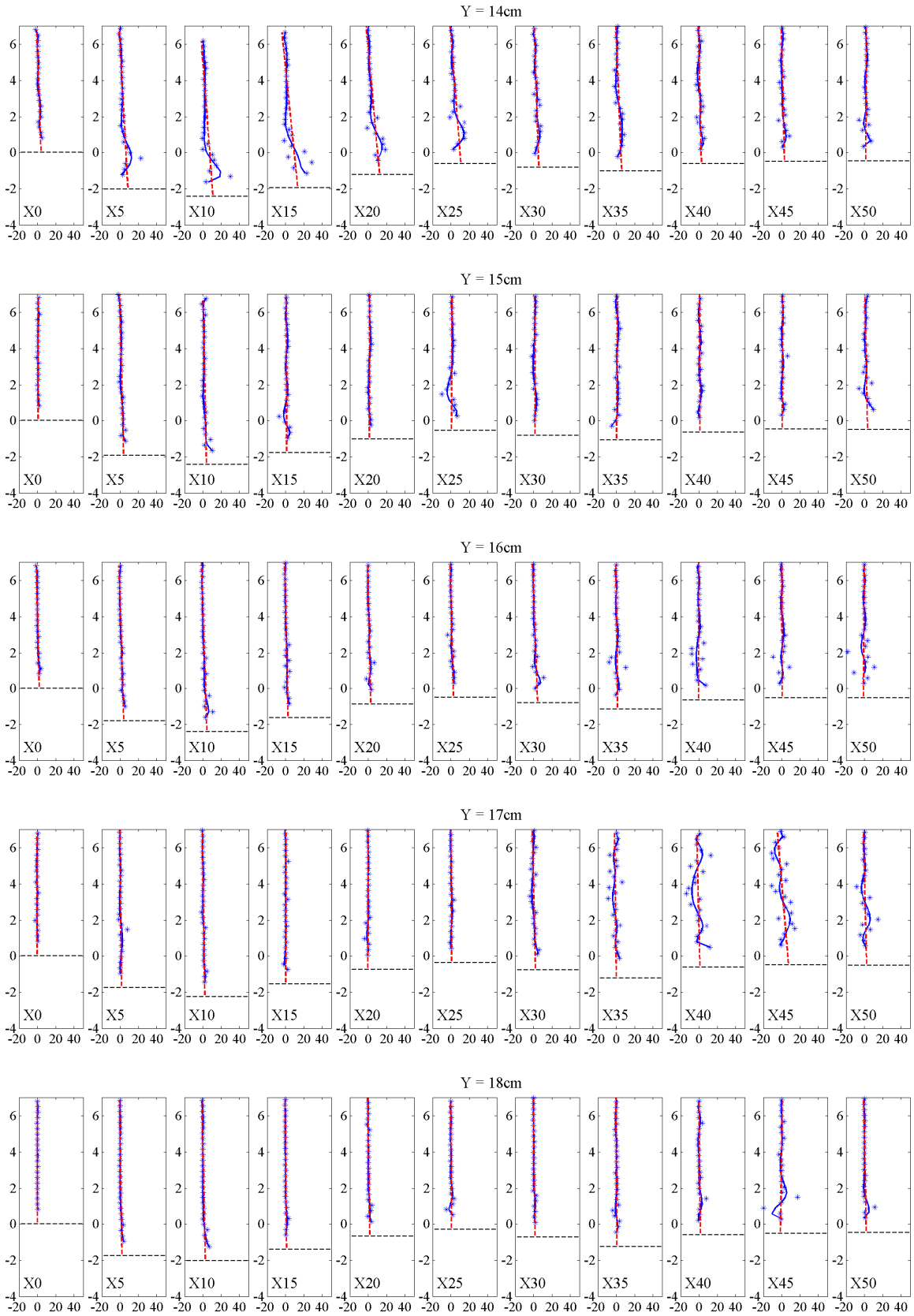

Figure 7.6 – Vertical distributions of the Reynolds stress (N/m^2): c) 14cm < Y < 18cm.

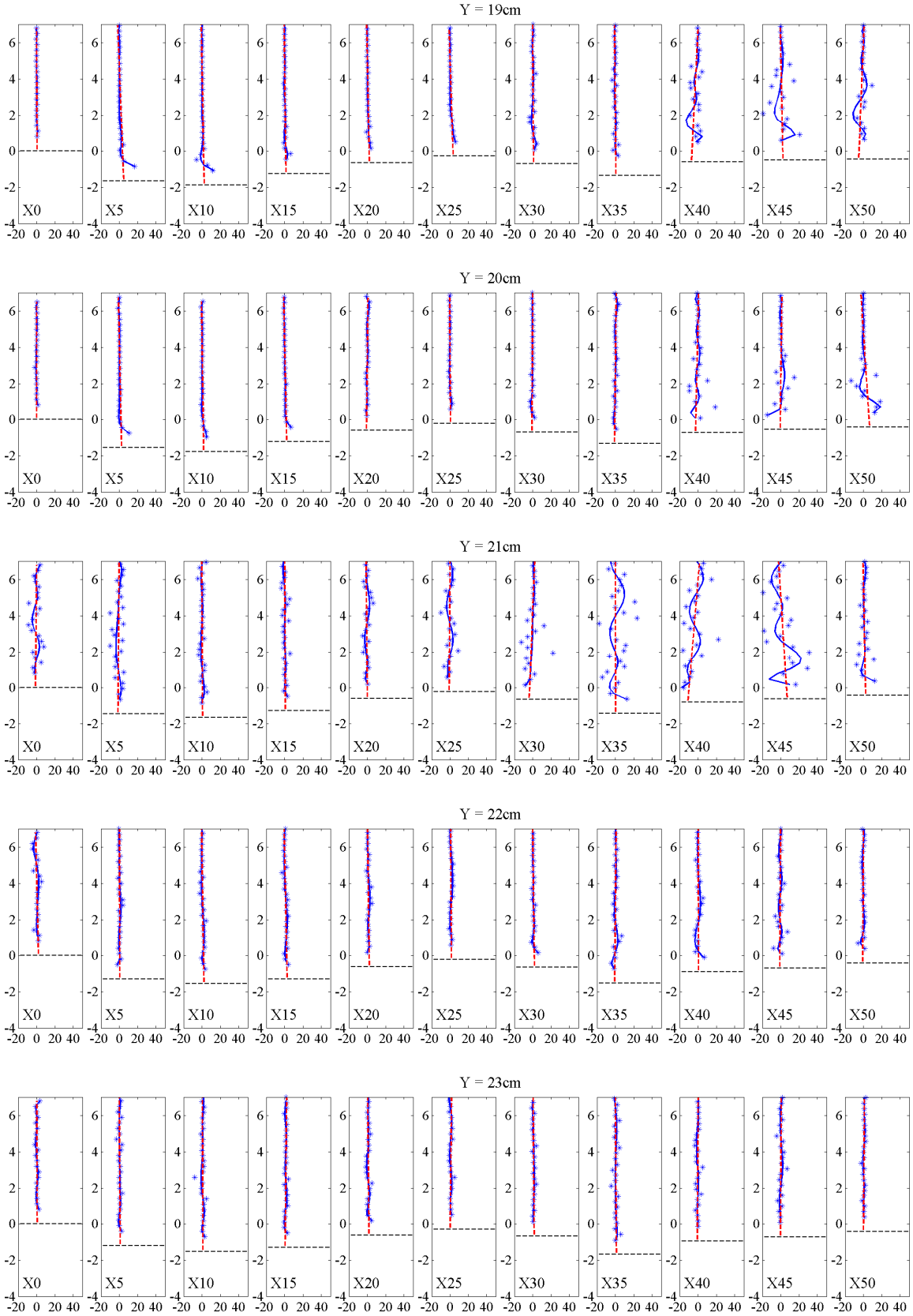

Figure 7.6 – Vertical distributions of the Reynolds stress (N/m^2): d) 19cm < Y < 23cm.

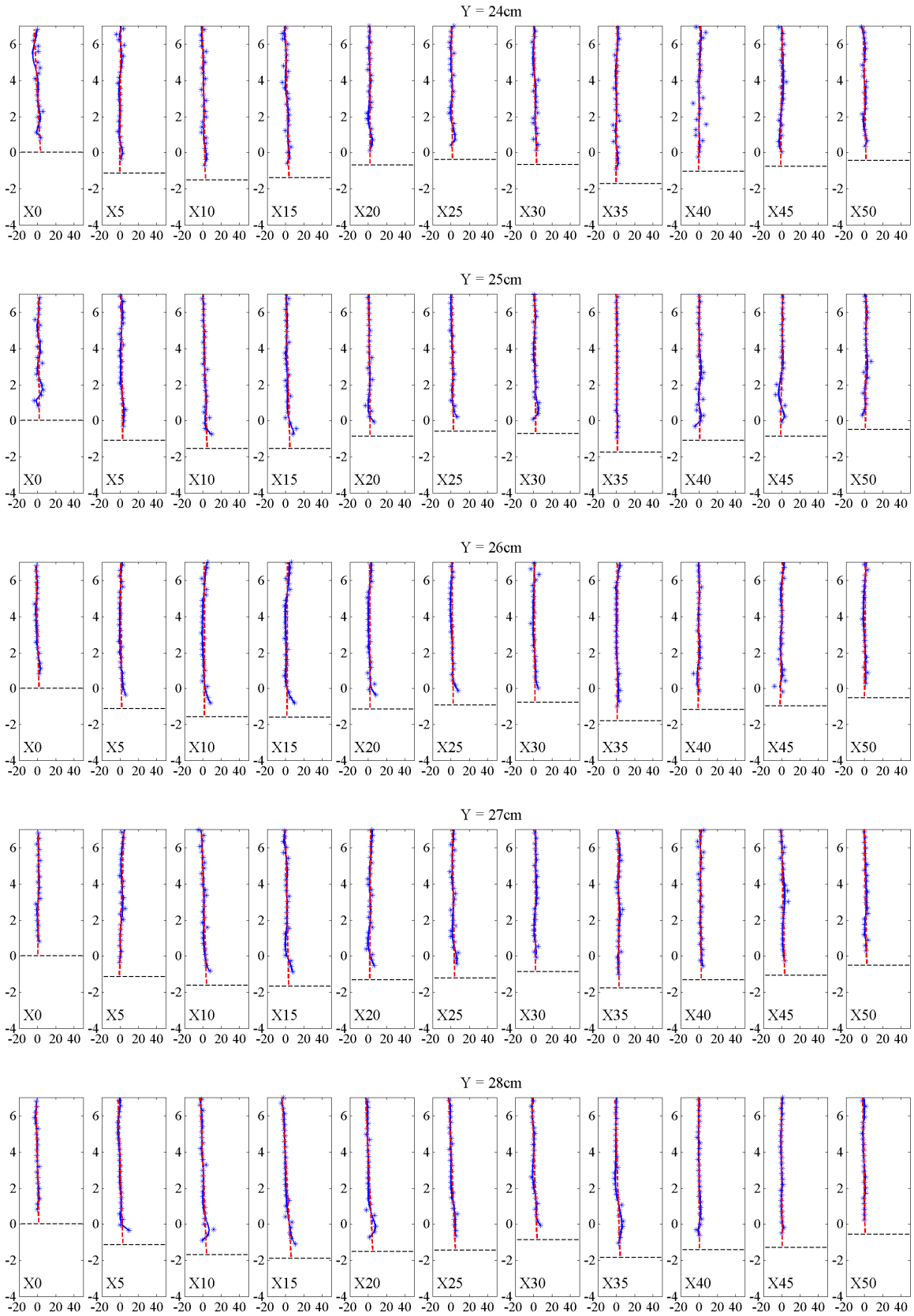

Figure 7.6 – Vertical distributions of the Reynolds stress (N/m^2): e) 24cm < Y < 28cm.

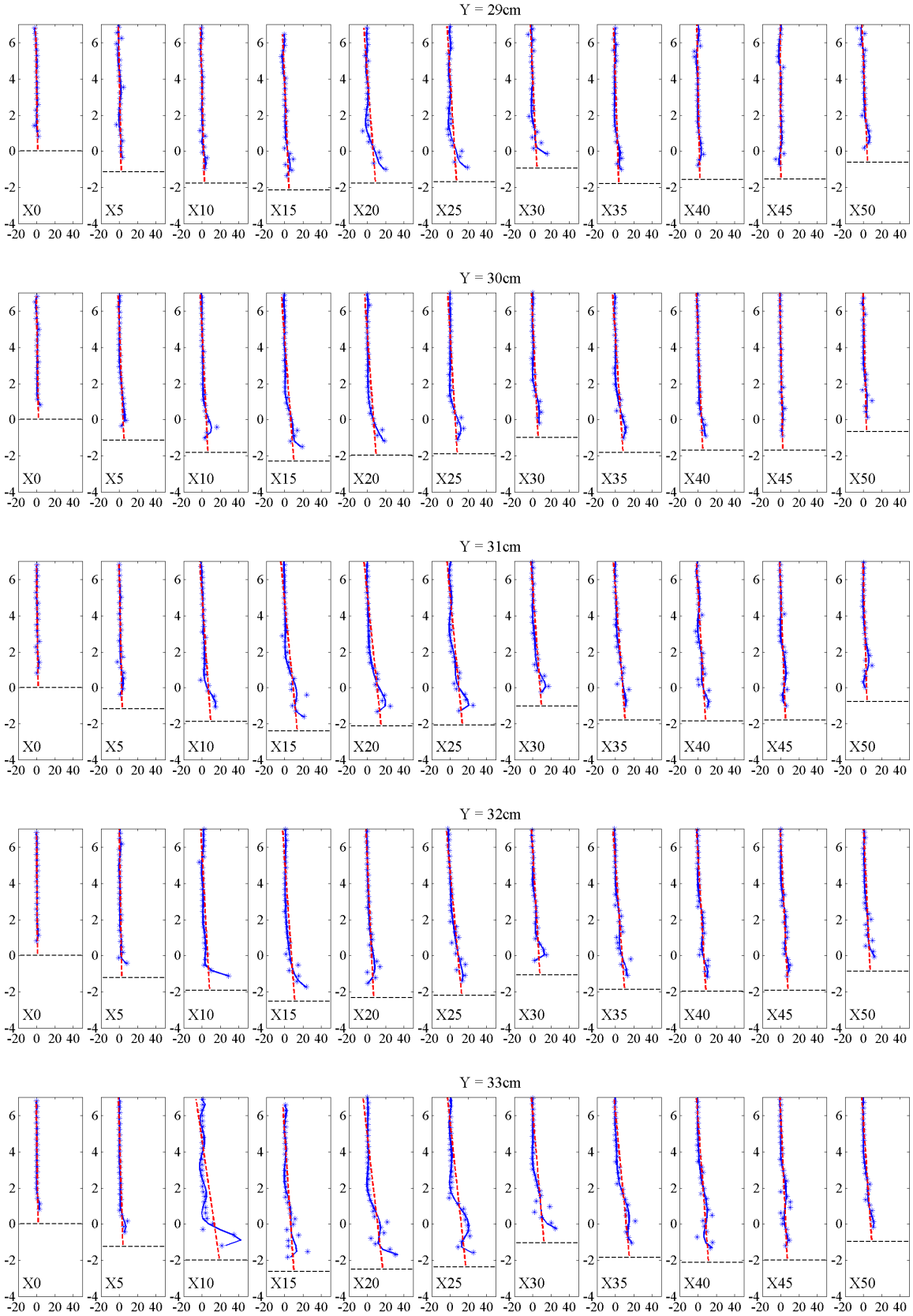

Figure 7.6 – Vertical distributions of the Reynolds stress (N/m^2): f) 29cm < Y < 33cm.

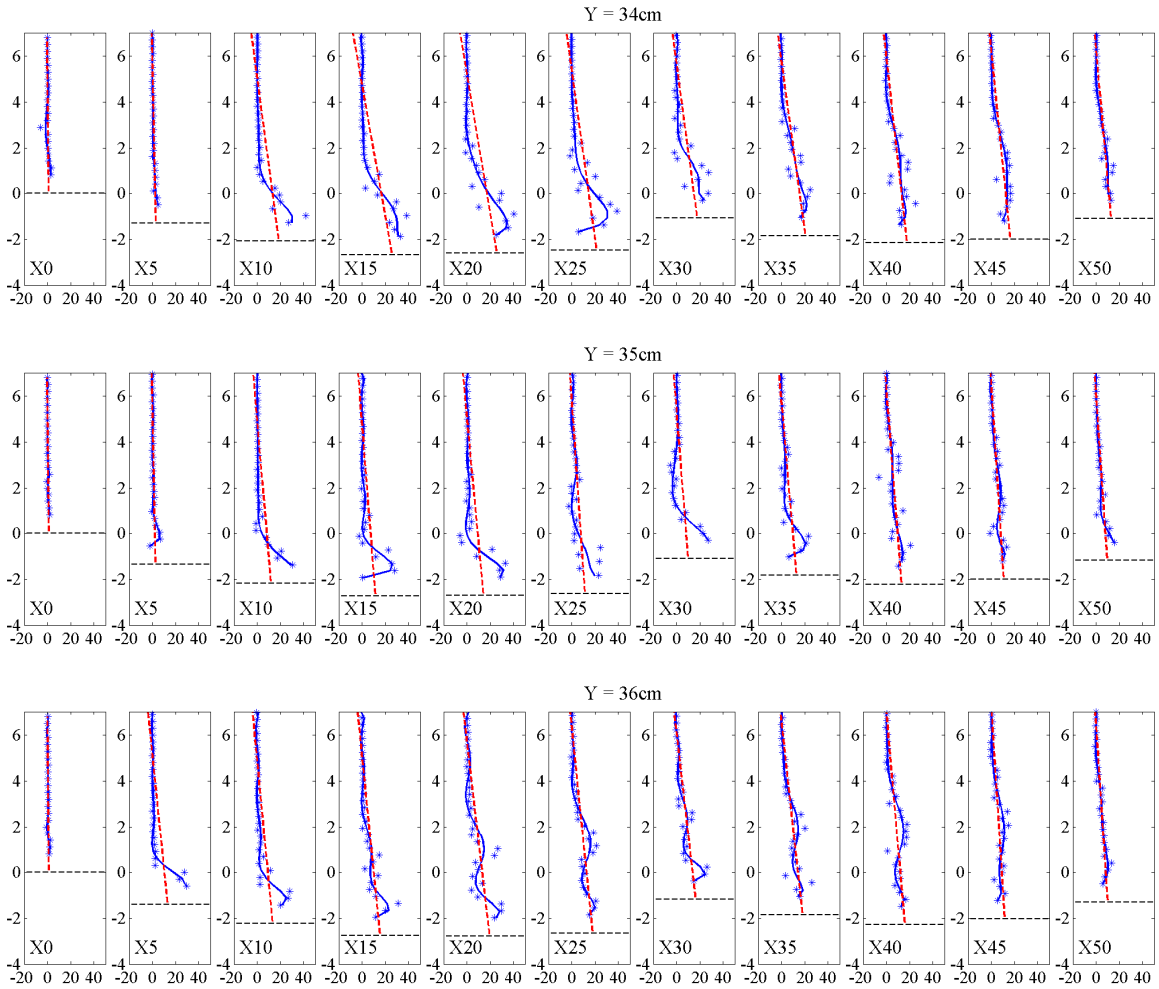

Figure 7.6 – Vertical distributions of the Reynolds stress (N/m^2): g) 34cm < Y < 36cm.

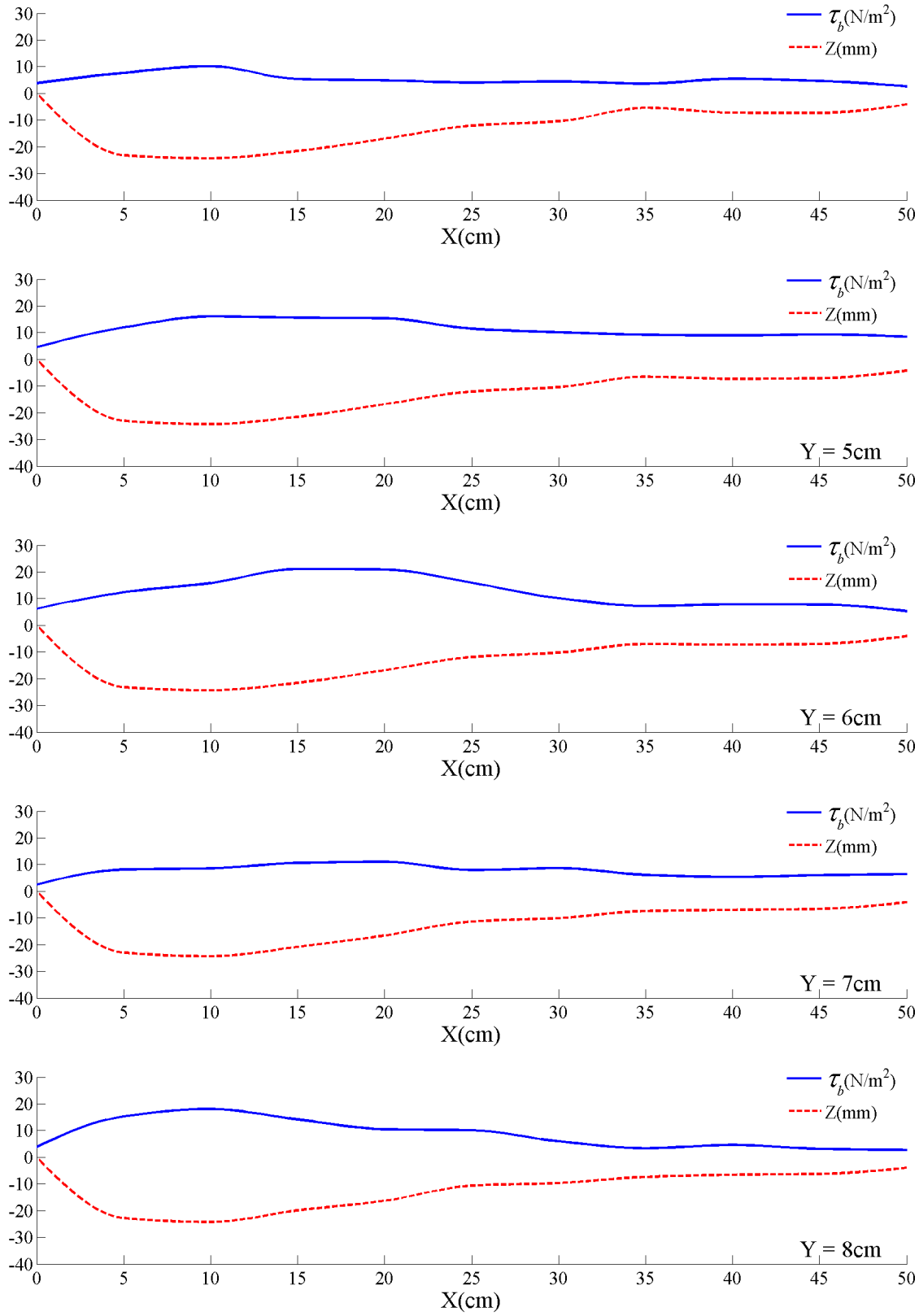

Figure 7.7 – Longitudinal distributions of τ_b (N/m^2): a) 4cm < Y < 8cm.

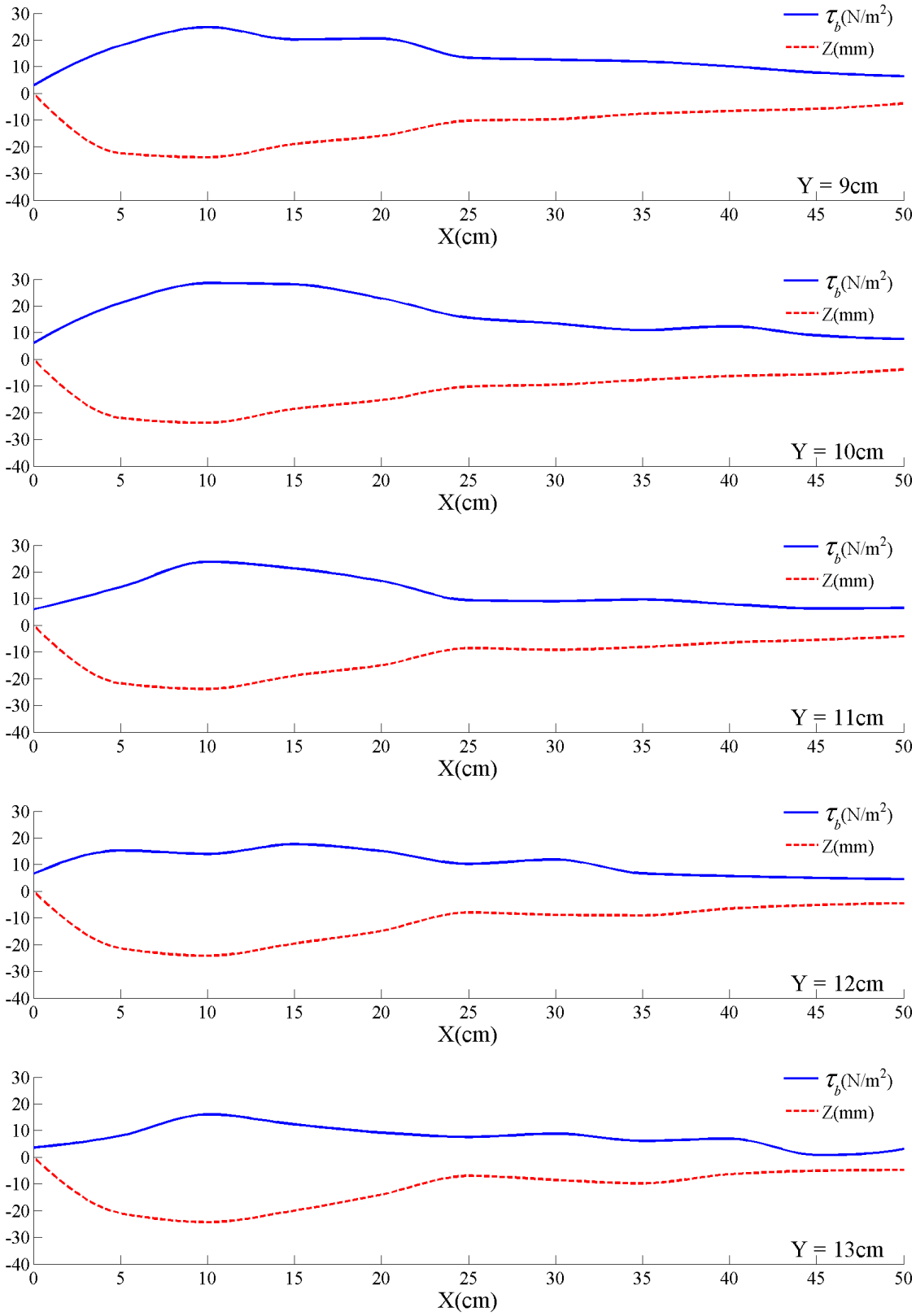

Figure 7.7 – Longitudinal distributions of τ_b (N/m^2): b) 9cm < Y < 13cm.

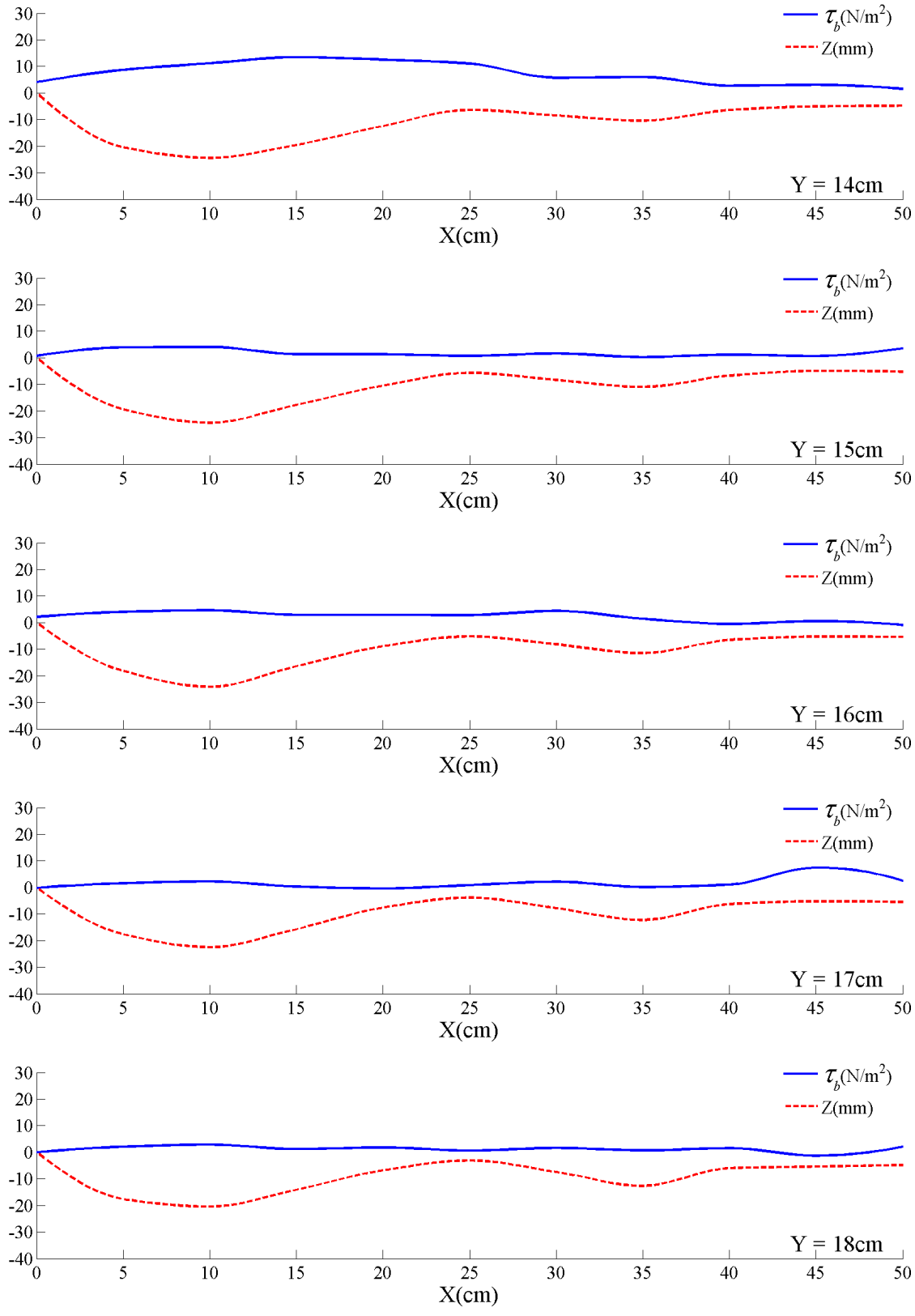

Figure 7.7 – Longitudinal distributions of τ_b(N/m^2): c) 14cm < Y < 18cm.

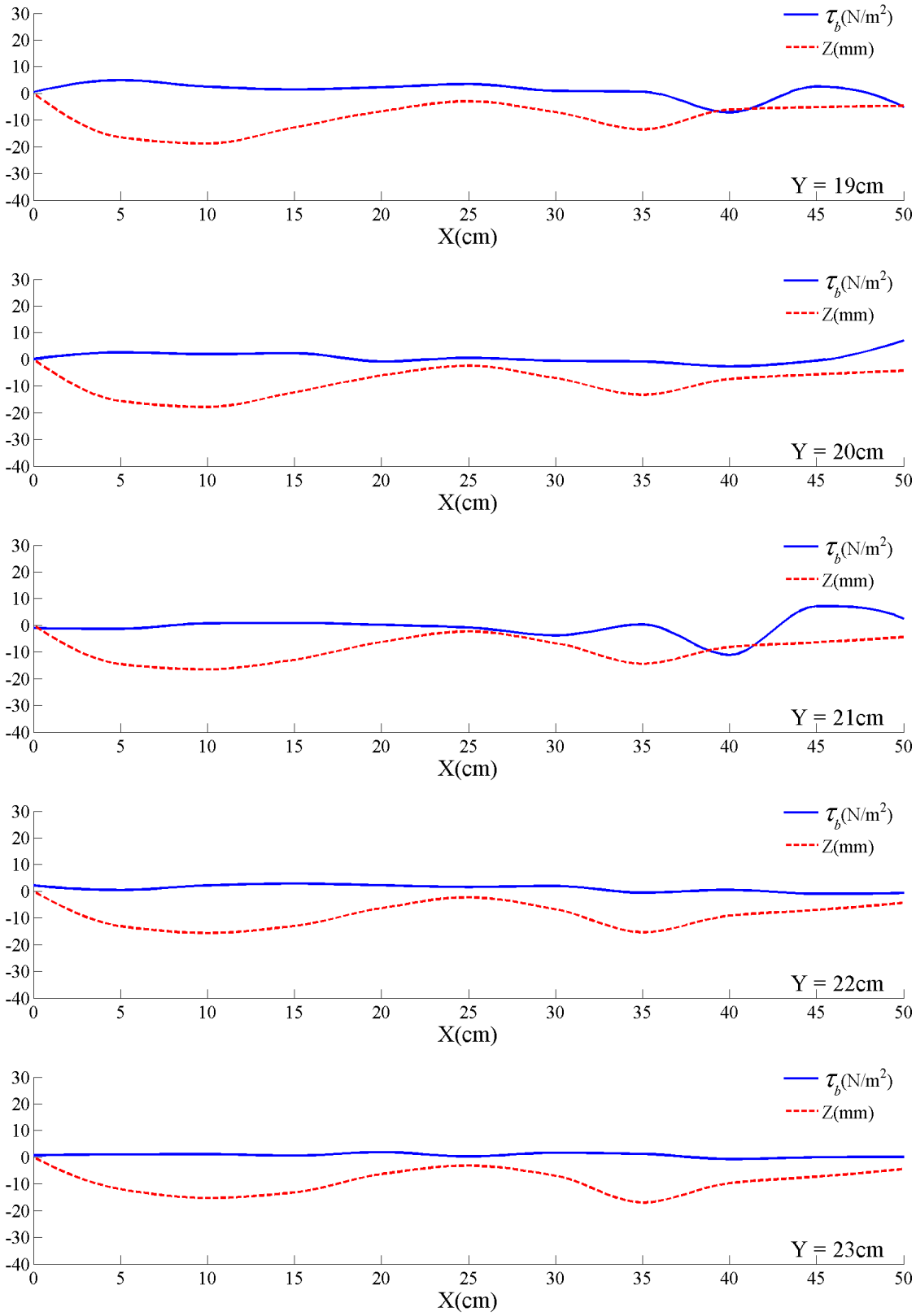

Figure 7.7 – Longitudinal distributions of τ_b (N/m^2): d) 19cm < Y < 23cm.

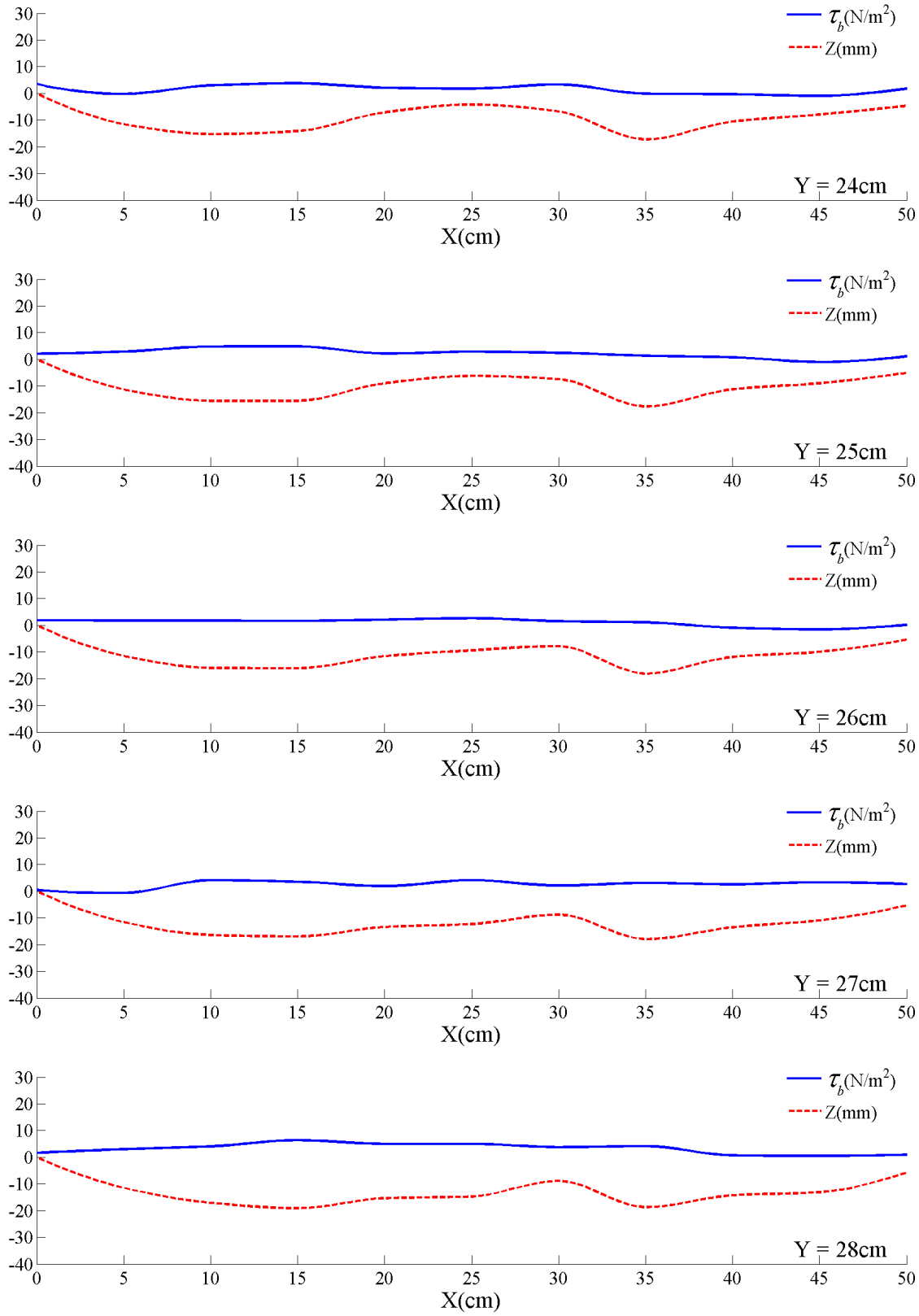

Figure 7.7 – Longitudinal distributions of τ_b(N/m^2): e) 24cm < Y < 28cm.

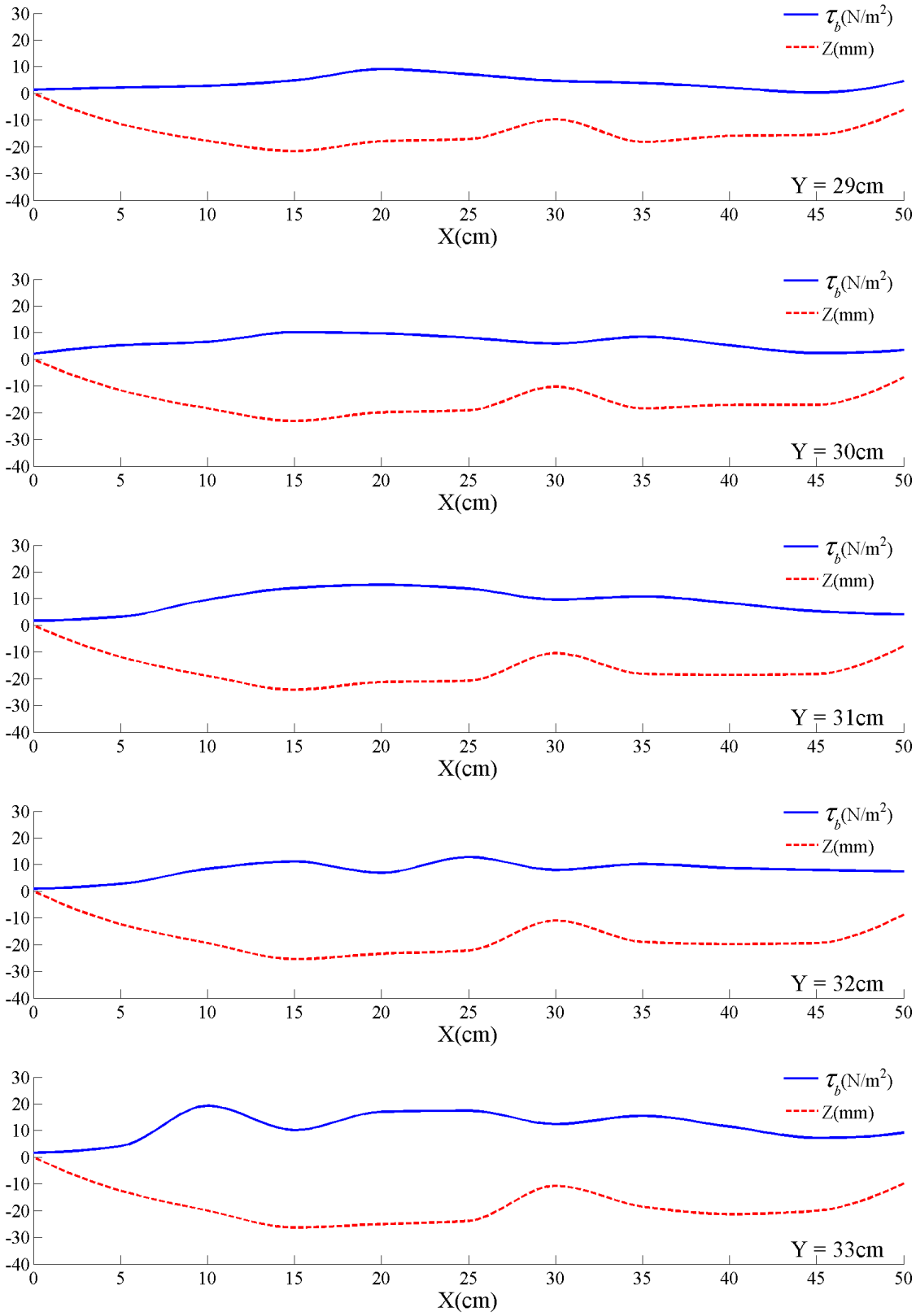

Figure 7.7 – Longitudinal distributions of τ_b (N/m^2): f) 29cm < Y < 33cm.

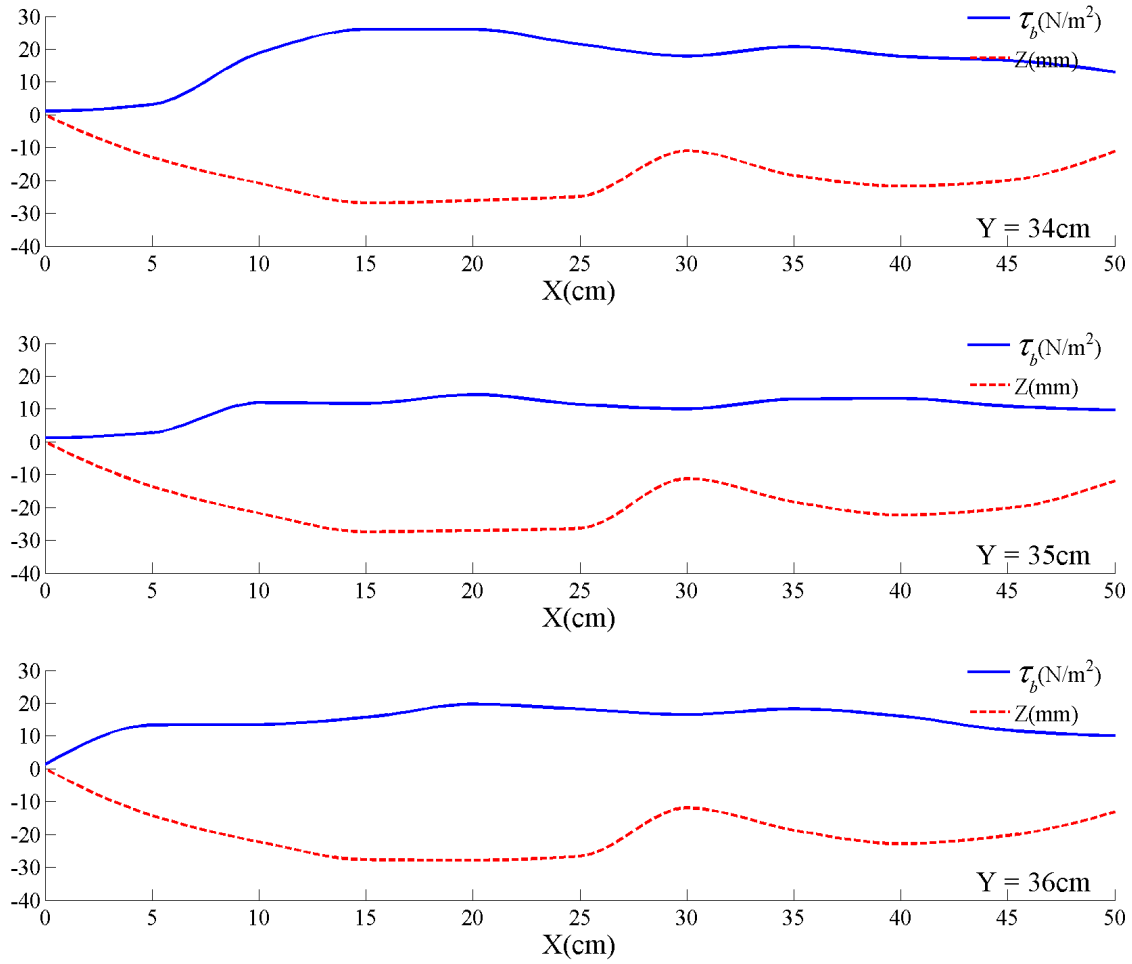

Figure 7.7 – Longitudinal distributions of τ_b (N/m^2): g) 34cm < Y < 36cm.

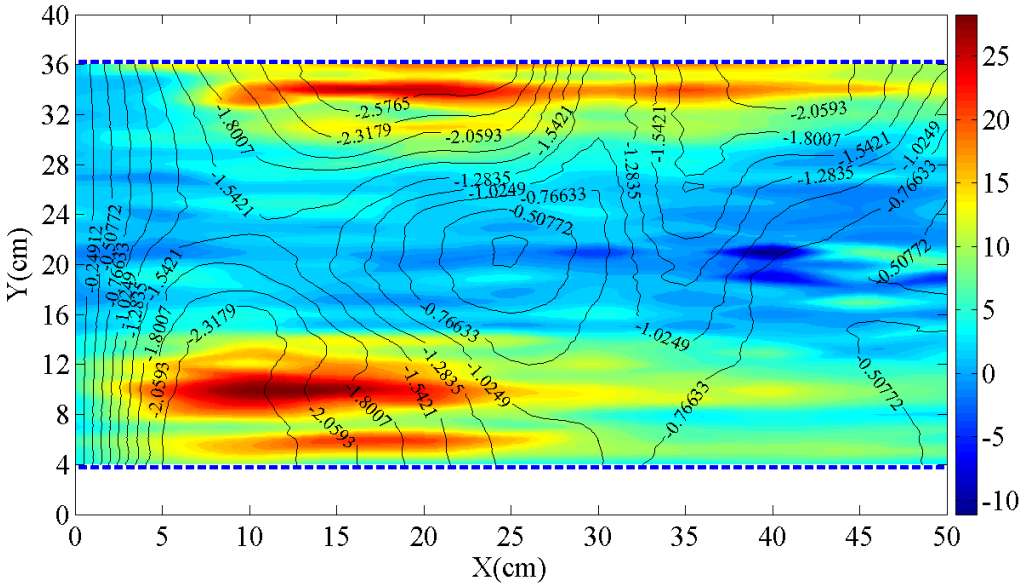

Figure 7.8 – Contour map of the bed shear stress τ_b (N/m^2).

In Figure 7.9 the estimated values of the bed shear stress τ_b are compared to with the measured ones τ_m (being τ_m equal to the Reynolds momentum flux determined near the bed by using the experimental data). The figure shows that the points in the plane τ_m - τ_b are generally distributed around the bisector line, with exception of the zone of higher values, where the shear stresses are underestimated. Furthermore, the linear regression of the data set gives a coefficient R^2 equal to 0.81.

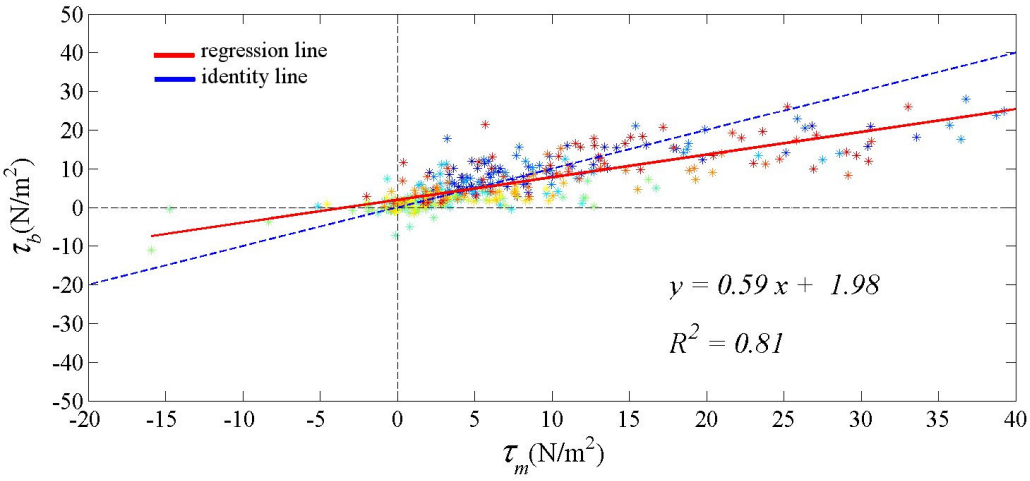

Figure 7.9 – Scatter plot of the couples[τ_m , τ_b].